Spatial and Temporal Variations in Mesoscale Water Vapor Retrieved from TOVS Infrared Radiances in a Nocturnal Inversion Situation

DONALD W. HILLGER[1]

Department of Atmospheric Science, Colorado State University, Fort Collins, CO 80523

(Manuscript received 30 July 1983, in final form 6 February 1984)

ABSTRACT

Mesoscale moisture fields are retrieved from TOVS (TIROS Operational Vertical Sounder) infrared radiances from two polar-orbiting satellites. A special feature of the retrieval process is the determination of the surface skin temperature independently of the temperature profile above the surface. This allows temperature inversions in retrieved temperature profiles, thereby more closely matching rawinsonde (RAOB) temperature profiles in inversion situations. A modification to the moisture feedback equation is required for such surface temperature inversion cases. Resulting satellite-derived total moisture values are compared both to RAOB-measured moisture at the RAOB scale (>250 km) and to total moisture estimated from surface dew points at the surface weather observation scale (<250 km). One finding is that mesoscale features are detected by the increased density satellite measurements which remain undetected by observations at the RAOB scale. Secondly, differences between satellite-derived and surface-estimated total moisture can indicate vertical moisture extent. Finally, time-changes in the satellite-derived total moisture fields are shown to be similar in pattern to moisture changes estimated from surface observations. Verification of such temporal changes can be found both in comparison to surface-estimated total moisture and by advection of moisture by the 700 mb wind.

1. Introduction

The retrieval of meteorological parameters from TOVS (TIROS Operational Vertical Sounder) measurements has been accomplished by several groups and has been documented in the published literature. However, most of these studies have dealt mainly with satellite temperature retrieval capability. The main emphasis of this work is the moisture retrievals, on which the published results are fewer. (In this paper, "moisture" refers to vapor-phase water only.)

Moisture tends to vary rapidly on small space and time scales and thus requires high space and time resolution. Wark *et al.* (1974) did some of the first mesoscale moisture analyses using high-resolution satellite measurements. Smith *et al.* (1979a) also analyzed moisture at the mesoscale. However, most previous work has dealt with synoptic-scale retrievals and comparisons to the RAOB network.

Gruber and Watkins (1979) determined that total column precipitable water was "reasonably well represented" by the TOVS retrievals. Their results included a rms precipitable water difference (compared to RAOBs) of 6 mm, or about 27% of a mean value of 23 mm. They pointed out, however, that moisture data at individual levels were at best marginal. This result is due to both the layered structure of the atmosphere and the inherently low vertical resolution of the satellite sounder. However, Hayden *et al.* (1981) showed that strong horizontal moisture gradients can be clearly defined by the TOVS measurements which are consistent with conventional observations. Moyer *et al.* (1978), using HIRS-1 (High-Resolution Infrared Radiation Sounder) data, achieved an rms dew point temperature difference of 7.3 K for all levels and stations for a single pass of HIRS-1 retrievals. This was a large difference for retrieved moisture at any single level, but when the moisture was analyzed in terms of integrated precipitable water the discrepancy was 2.6 mm of H_2O which represented only 20% of the total precipitable water.

In this study moisture parameters are retrieved from single satellite views at the same resolution as the synoptic surface observations. The surface observations come close to matching the high-resolution capabilities of satellite soundings even though the surface observations typically have a mean separation of at least 100 km. A point which must be stressed is that the synoptic surface observations of temperature and dew point were used in this study only for comparison to similar satellite-derived parameters.

Besides obtaining satellite soundings at the mesoscale (below 250 km), this study is an attempt to obtain high *time* resolution using HIRS-2 data. The time resolution of HIRS-2 is limited by the polar-orbiting satellite platform, but it gives a hint at the capabilities of

[1] Present affiliation: Cooperative Institute for Research in the Atmosphere (CIRA), Colorado State University, Fort Collins, CO 80523.

satellite soundings which can be obtained from geosynchronous orbit (Smith *et al.*, 1981; Chesters *et al.*, 1982).

The retrieval of moisture parameters from satellite measurements is generally more difficult than the retrieval of temperature parameters. This is true because water vapor is a highly variable absorbing and emitting constituent which causes strong changes in H_2O channel weighting functions. In the case of temperature retrievals the absorbing constituent, CO_2, has a relatively constant mixing ratio throughout the atmosphere. The temperature is merely a characteristic of the absorber, so temperature variations leave the weighting functions largely unchanged. However, the effect which moisture has on the weighting functions must be considered in every step in the retrieval process in which the moisture changes.

Another degree of difficulty in retrieving moisture information from satellite measurements arises because the moisture lies largely near the surface, and meteorological parameters near the surface are typically harder to retrieve than those in the middle levels. Much of the difficulty arises because of the strong effect of the boundary or surface temperature upon the satellite radiances. To determine moisture the surface skin temperature must be either known or retrieved independently of the atmospheric channels. The retrieval scheme, therefore, allows the surface skin temperature to be determined from satellite window channels alone and to float free of the temperature profile above the surface.

2. Satellite data

The satellite data used in this study are measurements obtained from the infrared sounding channels on the TIROS-N polar-orbiting satellite series. These infrared channels are designed to probe the vertical temperature and moisture structure of the atmosphere by employing frequencies which vary greatly in their atmospheric absorption. One inherent drawback of infrared measurements is their inability to sound below clouds, so in this study no satellite retrievals were produced in cloudy situations.

The TOVS system (Schwalb, 1978; Weinreb *et al.*, 1981) consists of three instruments: 1) HIRS; 2) the Stratospheric Sounding Unit (SSU); and 3) the Microwave Sounding Unit (MSU). Only the HIRS-2 or infrared data were used in this study. The weighting functions (for a standard atmosphere) for the TOVS channels used in this study are shown in Fig. 2.1 (Smith *et al.*, 1979b). TIROS-N and NOAA-6, both of which carry the TOVS instrument, are polar-orbiting satellites with sun-synchronous orbits. TIROS-N has local 0400, 1600 equator crossing time and NOAA-6 has local 0800, 2000 equator crossing times.

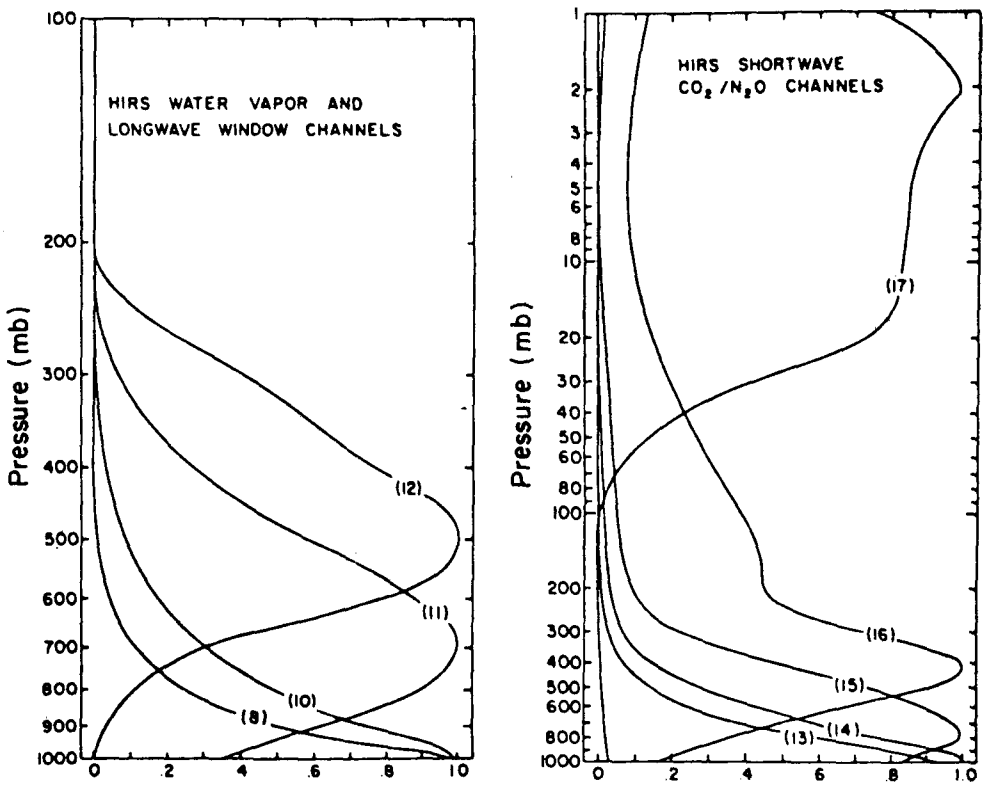

FIG. 2.1. Selected TOVS weighting functions [after Smith *et al.* (1979b)].

One of the periods when both TIROS-N and NOAA-6 were in synchronization, viewing nearly identical regions of the earth on successive passes, occurred on 30 September 1980. TIROS-N viewed the earth on a descending node (toward the equator) at approximately 1000 GMT (0400 LST) as shown in Fig. 2.2, and NOAA-6 followed a similar pattern (not shown) at approximately 1400 GMT (0800 LST). This 4-hour difference allows an examination of changes in the satellite-derived meteorological variables, especially moisture, during a small time span and at high spatial resolution. Data coverage was continuous along the satellite sub-track except for a calibration period every 40 scan lines. The calibration sequence lasts for a period equivalent to three scan lines, thereby skipping a swath about 120 km wide. A special objective analysis procedure has been developed elsewhere to interpolate into such calibration gaps when a continuous field is desired or is necessary (Lipton and Hillger, 1982).

Besides the infrared sounding channels, much higher resolution visible (1 km) and infrared (8 km) imagery from geosynchronous orbit was used to help determine when clouds were contaminating the satellite soundings. These Geostationary Operational Earth Satellite (GOES) images also give a good indication of the meteorological situation under study. Figure 2.3a shows the visible image at 1430 GMT 30 September 1980, which is one half hour past the 1400 NOAA-6 pass (henceforth all times are GMT unless otherwise stated). The central United States from Minnesota into Oklahoma is partly covered by a layer of fog. The GOES infrared image closest to the TIROS-N pass at 1000 is given in Fig. 2.3b. At this time little if any fog is indicated, but portions of the region that later produce fog appear warmer (darker) than the surrounding clear areas. One explanation for this warm appearance relative to surrounding areas is that the latter areas are drier and not as radiatively insulated, thereby allowing a stronger nocturnal cooling to take place (Parmenter, 1976). These dry areas show strong thermal inversions in the 1200 RAOB data.

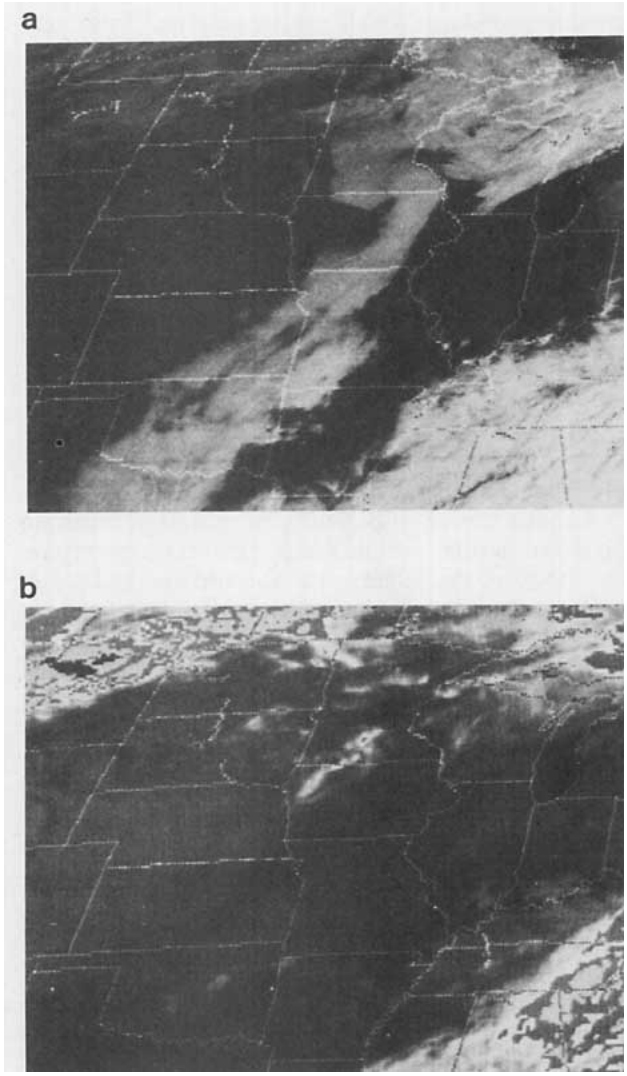

FIG. 2.3. GOES images for (a) 1430 (visible) and (b) 1000 GMT (infrared) 30 September 1980.

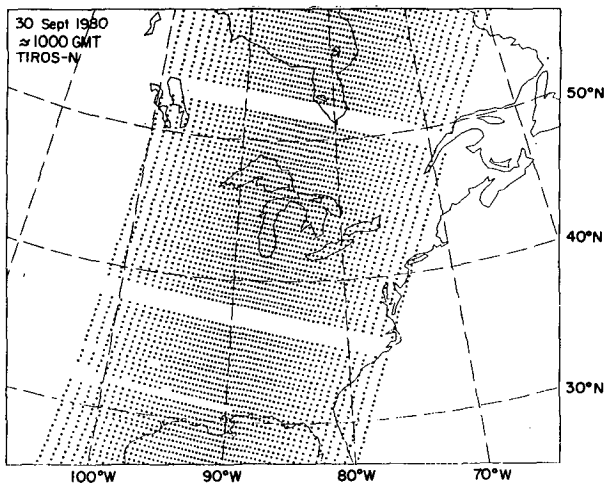

FIG. 2.2. TIROS-N descending orbit (equatorward) for ~1000 GMT (0400 LST) 30 September 1980. HIRS-2 sounding positions are shown.

3. Conventional data

Two sources of conventional data were used: 1) rawinsonde soundings (RAOBs), and 2) surface weather observations. The rawinsondes were used mainly to provide the initial guess temperature and moisture profiles for the iterative satellite retrieval system. Because the rawinsondes were the only source of conventional upper-air data, they were also used for comparison to the satellite-derived upper-air parameters at the synoptic scale.

The only RAOBs taken during the time period under consideration were the 1200 observations, midway between the two satellite sounding times of 1000 and 1400. This places the RAOBs within 2 hours of the satellite measurements. The RAOBs outlined by the solid box in Fig. 3.1 were averaged to provide the starting temperature and moisture profiles for the iterative retrieval process. (The dashed box is the area where the higher-density satellite retrievals were later performed.) Of the 27 RAOBs which went into the composited initial guess, all but Fort Sill, Oklahoma (FSI) are part of the NWS sounding network which has a typical spacing of at least 250 km.

There were some large differences among the individual soundings which went into the composited mean profile, especially with regard to the moisture and temperature structure near the surface. If the moisture profiles can be divided into three regimes, they would be characterized by 1) deep moisture, 2) a shallow moist layer near the surface with overlying dry air, and 3) relative dryness throughout the troposphere. Green Bay (GRB) and Salem (SLO), with deep moist layers from the surface to as high as 75 kPa (750 mb), are the moist extreme, whereas Topeka (TOP) and Fort Sill (FSI) typify the dry-over-moist situation with shallow moist layers of less than 10 kPa thickness (TOP sounding shown later). At the dry extreme are Omaha (3NO) and Amarillo (AMA). Other soundings displayed intermediate degrees of each of these three broad regimes.

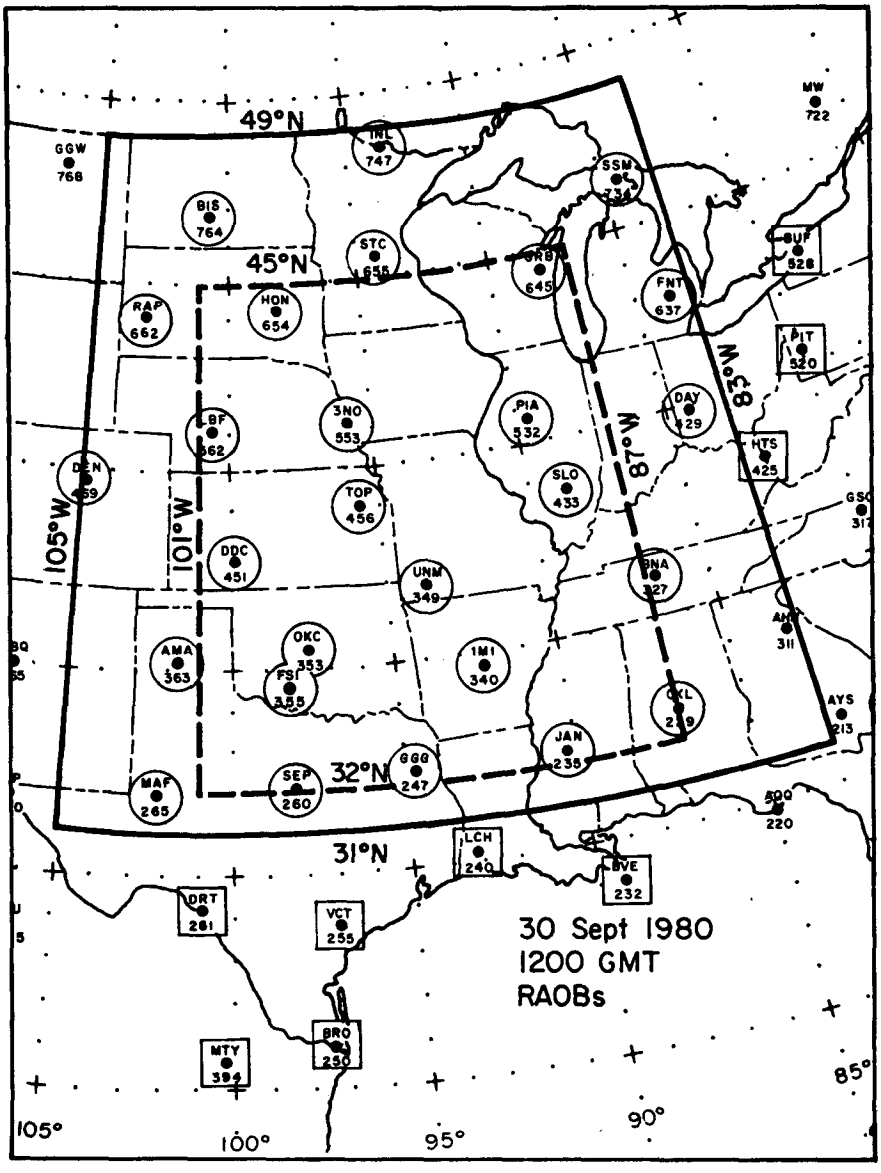

FIG. 3.1. Synoptic RAOBs taken at 1200 GMT 30 September 1980.

Many of the RAOB soundings contained shallow temperature inversions with temperature increases with height of around 10 K within the lowest 2 kPa. Soundings typical of these large temperature inversions occurred at North Platte (LBF) and Omaha. These inversions, however, were removed from the soundings when creating the composite temperature profile, because this one composite profile was used as the initial guess for all retrieved soundings at both 1000 and 1400.

The surface weather observations were used *only* for verification of the satellite-derived meteorological parameters at the surface observation scale. Surface observations were obtained at 0900, 1200 and 1500, the synoptic reporting times surrounding the TIROS-N and NOAA-6 satellite passes. Table 3.1 gives the number of reporting stations at each of the three synoptic times. The meteorological variables which were extracted from each of the synoptic surface stations were the temperature, dew point temperature and relative humidity. Since these three surface parameters are the only variables which were obtained at a density approaching that of the satellite data, they formed the basis for our satellite–conventional data comparisons.

In recent meteorological history there have been many attempts to use surface moisture measurements to estimate the total atmospheric water content. Reitan (1963) rekindled an interest in the relationship between surface dew point and precipitable water by using mean monthly values of both parameters to determine the coefficients a and b such that

$$\ln PW = a + bT_d, \qquad (3.1)$$

where PW is the precipitable water (mm) and T_d is the surface dew point (°C). His mean monthly values for 15 United States RAOB stations over a period of 3 years gave a correlation coefficient of 0.98, and the coefficients turned out to be $a = 2.413$ and $b = 0.061\ (°C)^{-1}$.

Bolsenga (1965), using the same relationship, derived coefficients of $a = 2.420$ and $b = 0.077\ (°C)^{-1}$ for 72 mean daily values with a correlation coefficient of 0.85, and $a = 2.243$ and $b = 0.069\ (°C)^{-1}$ for 97 hourly values with a correlation coefficient of 0.80. These results prompted Smith (1966) to conclude that "the longer the time period over which the mean values of water vapor content and surface dew point are formed, the more unique the relation is between these two variables".

TABLE 3.1. Synoptic surface observations (32–45°N, 87–101°W).

Time (GMT)	Number of observations
0900	101
1200	123
1500	126

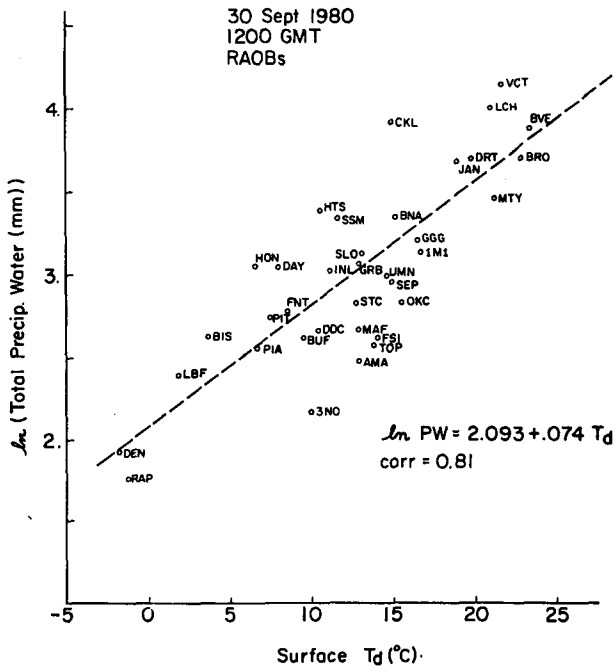

FIG. 3.2. Plot of total precipitable water versus surface dew point temperature for the 36 selected RAOB sites in Fig. 3.1. A linear least-squares regression line has been fit to the points.

In studying the temporal and spatial variability of precipitable water, Benwell (1965) found that "the observed value of precipitable water is not normally a good estimate of the value at that place 12 hours later." His study included 5 months of data from three Atlantic Ocean weather stations; his interest was in obtaining estimates of precipitable water based on higher-density surface observations over the ocean. He also concluded that the correlation coefficients between surface moisture and total water "are considerably higher than the autocorrelation coefficients over periods of 12 hours or more and seem likely to be higher than the autocorrelation for periods as short as six hours." In other words, it is better to estimate the precipitable water from surface moisture than to assume persistence for periods much longer than 6 hours.

It was thought to be possible to use the surface dew point measurements in this study to estimate the total precipitable water at a higher density than that of the synoptic RAOBs. First, the relationship of total water to surface dew point was established for the 1200 RAOBs as shown in Fig. 3.2. Points are plotted for 36 RAOBs as well as a least-squares line fit to those points. The 36 RAOBs include those from the 27 circled RAOB sites which went into the initial guess profile and nine other RAOB sites outlined by squares in Fig. 3.1. The extra RAOB sites to the south were especially helpful in establishing the regression line by supplying a set of moist soundings in the upper right corner of Fig. 3.2.

The equation for the regression line is given as

$$\ln PW = 2.093 + 0.074T_d. \quad (3.2)$$

The coefficients a and b are specific to this one date and time but are only slightly different than those given earlier. The correlation coefficient between the variables is 0.81 (66% explained variance). By eliminating a few outlying points the correlation can be increased, but the equation for the line remains almost unchanged.

Fig. 3.3a shows the RAOB-measured total precipitable water which ranges from less than 8 mm in western South Dakota and Colorado to over 40 mm in the southern parts of the United States. The differences between the RAOB and surface-estimated values, using Eq. (3.2), are shown in Fig. 3.3b. A large region of negative values extends from Texas into Minnesota. These are generally dry-over-moist situations where the surface-estimated total water values are greater than the actual values. This is also approximately the region where the fog forms. On the other hand, positive values show where the troposphere is moist through a large depth and occur to the east of the fog area. These differences, therefore, designate regions where the atmosphere is dry (−) or moist (+) aloft as indicated both by the RAOBs and the satellite images.

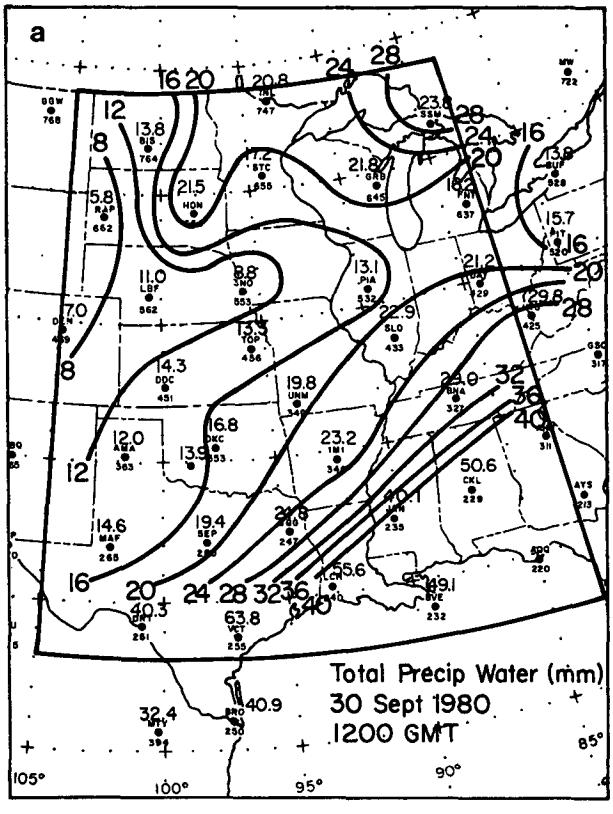

FIG. 3.3a. Total precipitable water (mm) from RAOBs at 1200 GMT 30 September 1980.

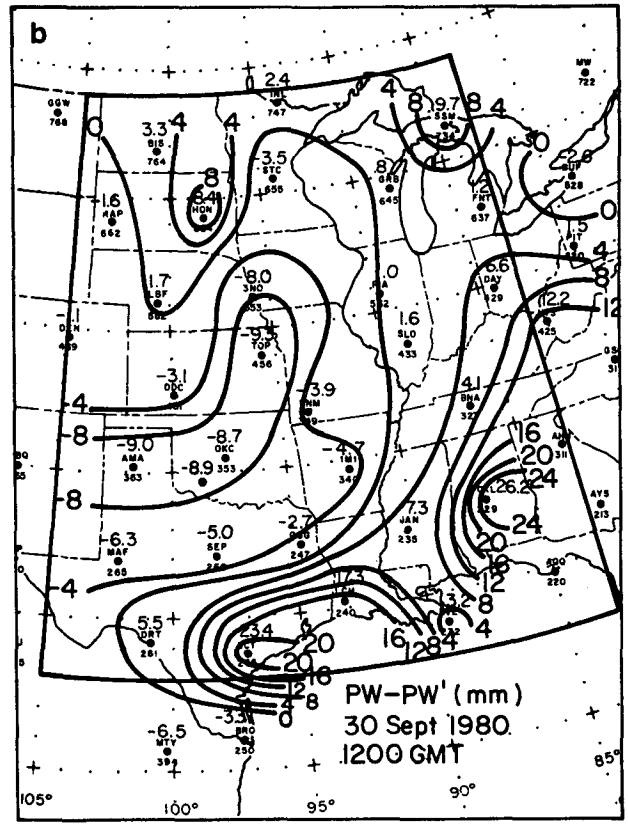

FIG. 3.3b. Precipitable water difference (mm) (measured minus estimated from surface dew point) for RAOBs at 1200 GMT 30 September 1980. The differences denote areas of dry (negative values) and moist (postive) aloft.

For comparison with retrieved moisture profiles it is necessary to assume a vertical distribution relating the total water to the surface mixing ratio. One such distribution is the power-law decrease in mixing ratio with pressure p,

$$Q(p) = Q_{\max}(p/p_{\max})^{\gamma}, \quad (3.3)$$

used in the Smith (1966) theoretical development, where $Q_{\max}$ is the surface or maximum mixing ratio at $p = p_{\max}$. When inserted into the precipitable water integral

$$U = g^{-1}\int_0^{p_{\max}} Q(p)dp, \quad (3.4)$$

where U is the precipitable water and g the gravitational acceleration, the result is

$$U = \frac{Q_{\max}p_{\max}}{g(\gamma + 1)}. \quad (3.5)$$

Inverting Eq. (3.5) results in

$$\gamma = \frac{Q_{\max}p_{\max}}{gU} - 1. \quad (3.6)$$

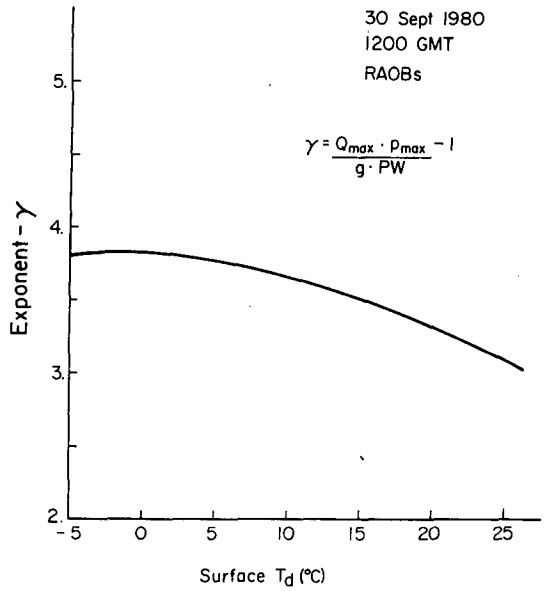

FIG. 3.4. Exponent for a power-law mixing ratio decrease with pressure as a function of surface dew point temperature. Results are based on Eq. (3.6) and precipitable water is determined by Eq. (3.2).

The exponent γ can then be found as a function of the surface mixing ratio or dew point temperature, and the total water U which is estimated from the surface dew point by using a relationship of the form of Eq. (3.1).

For the surface dew point to precipitable water relationship found for the 1200 RAOBs in Eq. (3.2), the exponent γ varies slightly with dew point as shown in Fig. 3.4. A mean value for γ of approximately 3.5 would represent most situations. This value can be used to construct an estimated moisture profile given only a surface dew point temperature and pressure. This technique will be used later for comparisons with satellite-derived moisture profiles.

4. TOVS retrieval system

The retrieval scheme used to obtain the high-resolution TOVS (HIRS-2) soundings is based on software similar to that used previously for HIRS-1 data (Hillger and Vonder Haar, 1981). Modifications were introduced to accomodate particular problem areas presented by this study.

First, retrievals were done only under clear conditions, so the cloud problem was reduced to detection and elimination of cloud-contaminated soundings. After cloud elimination, the next step was to correct the shorter wavelength infrared channels which are susceptible to reflected solar radiation. This was only necessary for the 1400 pass from NOAA-6. The correction technique used is similar to that used by Hayden *et al.* (1981).

Second, a special problem was introduced by the existence of strong surface temperature inversions in this data set. To deal with this problem a temperature inversion had to be introduced into many of the nighttime retrieved temperature profiles to produce a meteorologically and physically reasonable solution to the radiative transfer equation.

Next, a terrain height correction was necessary because the satellite retrievals covered a large area where terrain elevations varied greatly. Surface pressures were estimated using the hydrostatic relationship and mean terrain elevation data for the area under study (Hillger, 1983).

Finally, the interactive moisture feedback mechanism, which allows feedback to the moisture profile, required modification for noctural inversion situations.

a. Cloud detection

The technique used for cloud detection depended on the time period under study. For the 1400 (after sunrise) satellite data the cloud detection was simplified by a visible window channel at 0.69 μm. The visible reflected radiance was not examined directly, but as a fraction of its maximum possible value (assuming reflectance = 1.0). This was called the bi-directional reflectance (percent). A value of 40% was used as the cloud–no cloud threshold, with larger values of reflectance due to clouds.

An alternate means of cloud detection utilized the window brightness temperature difference (WBTD) between the 3.7 and 11 μm window channels. (The brightness temperatures at 3.7 and 11 μm are not corrected for atmospheric attenuation.) This value is plotted and contoured in Fig. 4.1. Shading is used to designate values greater than 10 K and matches well the cloudy area shown in the visible image in Fig. 2.3a. Small brightness temperature differences occur in the clear areas. The large WBTD values are due to both reflected visible radiation at 3.7 μm (none at 11 μm) and different amounts of atmospheric absorption of these two wavelengths. (The 3.7 μm channel typically has a larger brightness temperature than the 11 μm channel because of lower atmospheric absorption.) The reflected radiation effect is dominant during the day, so large brightness temperature differences can be used to detect clouds.

A plot of the WBTD values versus the bi-directional reflectance is given in Fig. 4.2 and shows a strong relationship. Soundings with both values below their respective thresholds of 10 K and 40% are most likely clear. Those above both thresholds are most likely cloudy. Others are possibly either partly cloudy (WBTD $>$ 10 K but bi-directional reflectance $<$ 40%) or possibly completely cloudy with a uniform cloud top (bi-directional reflectance $>$ 40% but WBTD $<$ 10 K).

At night the cloud detection is hindered by the lack of reflected visible radiation. However, the WBTD values can still be used. Since the visible radiation component at 3.7 μm is gone, the WBTD values are reduced

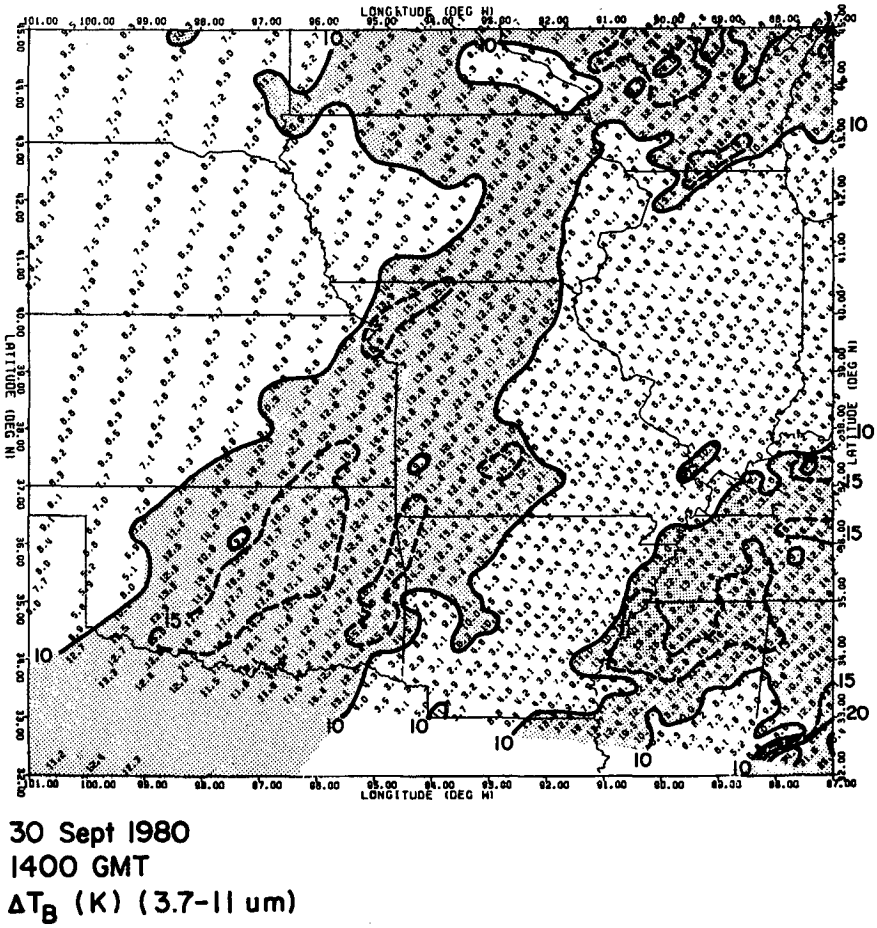

FIG. 4.1. Window brightness temperature difference (K) (3.7–11 μm) at 1400 GMT 30 September 1980.

and may even be negative due to variations in the surface emittance. By comparing the nighttime WBTD values (not shown) to the nighttime infrared cloud image in Fig. 2.3b it appears that values greater than approximately 4 K are due to clouds and are thus rejected.

So, by using differences between two window channel measurements, most cloudy situations can be detected both during the day and at night. Thin or small clouds, however, can remain undetected. With most cloudy values eliminated, temperature and moisture profiles can be retrieved by assuming clear column conditions.

b. Nocturnal surface temperature inversions

During the nighttime or early morning hours nocturnal cooling can allow a temperature inversion to develop near the surface. This temperature inversion is typically shallow and is not easily sensed by satellite measurements. Paulson and Horn (1981) recognized and warned of the nocturnal inversion problem in the retrieval of temperature profiles from Nimbus-6 HIRS radiances. As a result, a nocturnal inversion is allowed when it is implied by the window channel radiances.

The first step in determining whether a temperature inversion exists is to look at the surface skin temperature implied by the three window channels at 3.76, 3.98 and 11 μm. In clear, dry situations these three window channels typically give very similar brightness temperatures. The maximum of these three window brightness temperatures, after correcting the shorter wavelength windows for reflected solar radiation, is used as the surface skin temperature for the initial guess temperature profile which is a composite of 1200 RAOBs. A temperature inversion (temperature reduction) at the surface is allowed as the first step in the retrieval process if the maximum window brightness temperature for a particular spot is lower than the air temperature at the surface given by the initial guess profile. In a similar manner, if the maximum window channel brightness temperature at another position is larger than the initial guess surface air temperature, the surface skin temperature is increased,

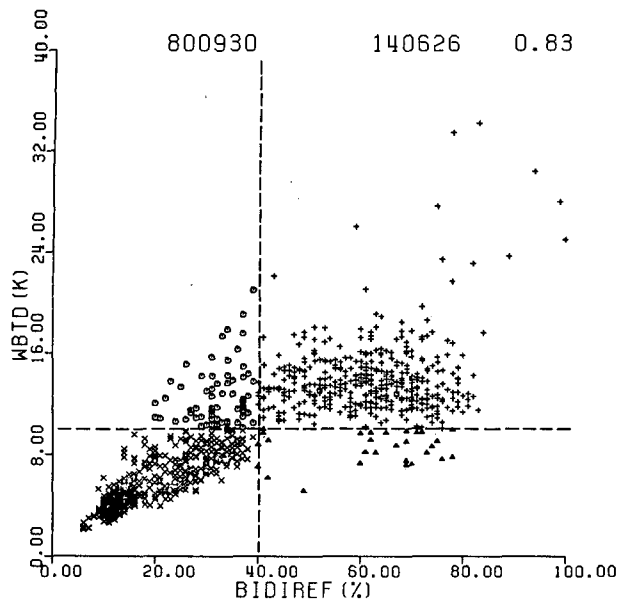

FIG. 4.2. Scatter plot of window brightness temperature difference (3.7–11 μm) versus bi-directional reflectance for the area from 32–45°N, 87–101°W, for the 1400 GMT 30 September 1980 satellite pass. A correlation coefficient of 0.83 is given.

thereby allowing a larger lapse rate or even possibly allowing a superadiabatic layer to be represented near the surface.

Using the maximum window channel brightness temperature to determine the surface temperature for the initial guess profile has the effect of allowing the surface skin temperature to float free of the atmospheric temperature profile. This seems appropriate in situations where the surface skin temperature can vary greatly in space and time. This also allows the same initial guess profile to simulate lapse rates near the surface which range from inversion to superadiabatic, especially when the layer is shallow as is true in the cases examined. As a result, vertical temperature detail can be added near the surface as required. However, the thickness of this lowest layer is limited by the distance between the lowest (non-surface) retrieval level and the surface.

An example of an added surface temperature inversion is shown in Fig. 4.3. The Huron South Dakota (HON) sounding at 1200 30 September 1980 is shown to have a strong but shallow temperature inversion. The composite initial guess temperature profile is also shown as it is originally given but with an inversion as implied by the maximum window channel brightness temperature at 1000. The large discrepancy between the two surface temperatures may be due to their 2-hour time difference.

c. *Iterative feedback mechanisms*

The basic iteration loop for the TOVS (HIRS-2) retrievals uses the differences between the observed radiances and the radiances calculated for the initial guess profile as feedback to correct the initial guess sounding. Appropriate channels are used to feedback to the surface temperature, the moisture profile, and the temperature profile.

The surface temperature feedback is a modification of that used previously (Hillger and Vonder Haar, 1981). The modification is due to the use of three instead of two window channels in the surface temperature feedback. The feedback equation for iteration n becomes

$$T_{\text{sfc}}^{(n+1)} = \Big(\sum_{i=1}^{3} T_{i,\text{sfc}}^{(n+1)} \tau_{i,\text{sfc}}^{(n)}\Big)\Big(\sum_{i=1}^{3} \tau_{i,\text{sfc}}^{(n)}\Big)^{-1}, \quad (4.1)$$

where the $T_{i,\text{sfc}}^{(n+1)}$ are determined from the approximation

$$L(i, T_{i,\text{sfc}}^{(n+1)}) = L(i, T_{\text{sfc}}^{(n)}) + \Delta L_i^{(n)} (\tau_{i,\text{sfc}}^{(n)})^{-1}$$

and the inverse Planck relationship. The correction term is given by

$$\Delta L_i^{(n)} = L_{i,\text{obs}} - L_{i,\text{calc}}^{(n)}.$$

The new surface temperature is a weighted average of the temperatures suggested by each of the three

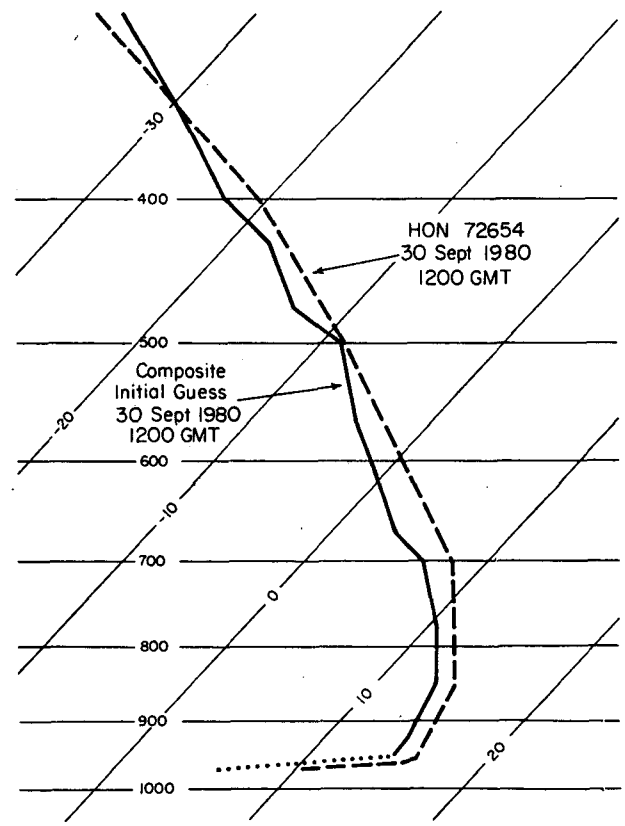

FIG. 4.3. An example of a surface temperature inversion added to the initial guess temperature profile by using the maximum window channel brightness temperature as a floating surface temperature.

window channels i, and the weights are the surface transmittances τ_i for each channel. The surface temperature suggested by each channel is based on the radiance difference (observed minus calculated) and is inversely proportional to the surface transmittance in that channel.

The moisture feedback requires special modification when applied in nocturnal inversion situations. The formula used to update the mixing ratio $Q(p)$ for iteration n at any pressure p is

$$Q^{(n+1)}(p) = Q^{(n)}(p)\left[1 - \frac{\sum_{i=1}^{3} S_i^{(n)} \Delta L_i^{(n)} \Delta \tau_i^{(n)}(p)}{\sum_{i=1}^{3} \Delta \tau_i^{(n)}(p)}\right], \quad (4.2)$$

where

$$\Delta \tau_i(p) = \tau_i(p_m) - \tau_i(p_{m+1})$$

is the weighting function for each of the H_2O channels and $S_i^{(n)}$ is the factor for converting from radiance change to mixing ratio change.

The S factors relate how the radiance in a given channel changes with the moisture profile. Typically the H_2O radiance decreases with increasing atmospheric moisture content. This is true because with increased moisture (or absorber) amount the transmittance of the atmosphere decreases and the resulting weighting function peaks higher in the atmosphere, or at cooler temperatures. Since more of the radiance arises from cooler portions of the atmosphere, the integrated radiance is reduced. The effect, however, is reversed if a strong temperature inversion exists, especially at the surface. The physical dimension of S is percent change in mixing ratio per change in radiance L (i.e., inverse radiance units). A more complete explanation of the calculation of the S factors is given in the Appendix.

The effect of surface skin temperature and air temperature differences on the radiance response to moisture variations is summarized in Fig. 4.4. Shown are brightness temperatures calculated for the three H_2O channels as a function of total atmospheric precipitable water, based on the United States standard atmosphere with T_{max} equal to the air temperature at the surface. The results of the surface skin temperature T_{sfc} modified by adding and subtracting 10 K from T_{max} are shown by the dotted and dashed lines, respectively. Channel 12 at 6.7 μm is virtually unaffected by the surface and shows, as a control, how the water vapor radiance (or brightness temperature) typically decreases with increasing moisture content. A similar effect occurs at 7.3 μm which has only a slight surface contribution. However, the most transparent H_2O channel at 8.2 μm changes its slope as a function of the surface temperature departure. For a 10 K increase in the surface temperature the "normal" effect of decreased

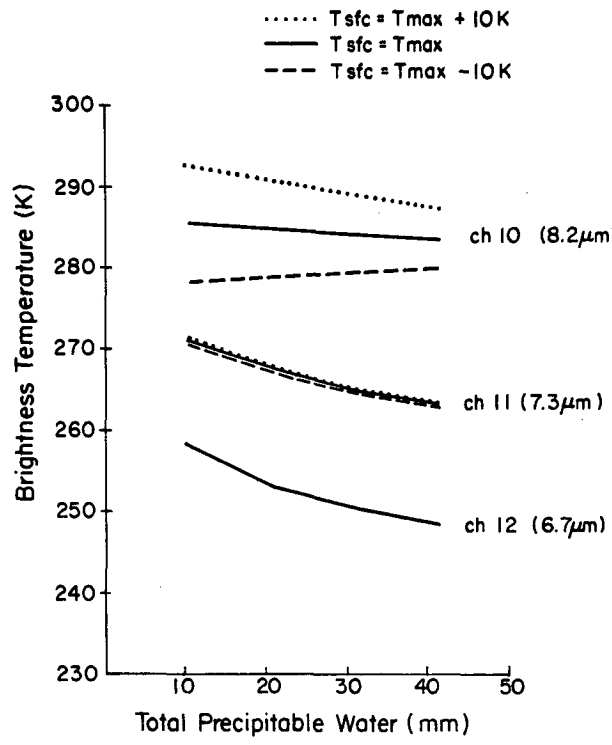

FIG. 4.4. Simulated brightness temperature response for the three H_2O channels as a function of the total atmospheric precipitable water and the surface temperature deviation from a given temperature profile.

radiance with increased moisture is more pronounced, but with a 10 K temperature inversion (decrease) at the surface the effect of changing moisture on the calculated radiance is *reversed* (the dashed line for Channel 10). In this case the S factor for this channel would be reversed in sign, to reflect the increase in radiance with increased moisture. The magnitude of S is initially calculated based on the guess temperature and moisture profiles and the initial surface skin temperature. The S factors are then updated before each moisture iteration based on the new temperature and moisture profiles and surface skin temperature.

Empirical evidence of the increase in radiance with increase in moisture under inversion conditions is given by Parmenter (1976). In nighttime infrared images, moist areas appear darker (warmer) than adjacent drier areas. This effect may be caused partly by the moist atmosphere acting as a blanket to keep the surface in that region warmer than in adjacent dry regions. Parmenter, however, notes that early morning surface heating quickly destroys this infrared pattern. Gurka (1976) also noted that moist areas appear warmer at night. His explanation pointed to the effect of the moist air upon the radiating surface causing variations in surface temperature, but he also said that the surface temperature measurements at instrument shelter height do not always confirm this radiative effect. It is possible

that the effect noted by these two authors is not entirely due to a surface temperature variation from moist to dry areas. In a surface temperature inversion situation the moist areas would appear warmer because of the increased absorption and emission from the higher, warmer layers.

Finally, the feedback for the temperature profile is accomplished using the relaxation formula for iteration n:

$$L[i, T^{(n+1)}(p)] = L[i, T^{(n)}(p)]\left[1 + \frac{\sum_{i=1}^{4} \Delta I_i^{(n)} \Delta\tau_i^{(n)}(p)}{\sum_{i=1}^{4} \Delta\tau_i^{(n)}(p)}\right], \quad (4.3)$$

where

$$\Delta I_i^{(n)} = (L_{i,\text{obs}} - L_{i,\text{calc}}{}^{(n)})/L_{i,\text{calc}}{}^{(n)}$$

is the normalized radiance difference. As with the moisture feedback, this difference is a function of the channel i and causes the maximum change in the temperature profile where the weighting function $\Delta\tau_i$ for that channel has its peak. For the temperature feedback only the four most transparent CO_2 channels were used because of the emphasis on lower-tropospheric moisture results.

The order of these feedback mechanisms alternates between the moisture and temperature profiles with the surface skin temperature feedback occurring before each change to the moisture or temperature profile. The surface temperature feedback is computed first and more often because of its strong effect on the radiative transfer equation. Each iteration cycle, therefore, consists of feedback to: in order, 1) the surface temperature; 2) the moisture profile; 3) the surface temperature again; and 4) the temperature profile. After each change in the moisture or temperature profile the transmittances are recalculated using software developed by NOAA/NESDIS personnel (Weinreb *et al.*, 1981). Iterations are continued until either three iteration cycles have passed or the radiance residual does not decrease. This residual is the rms difference between calculated and observed radiances for all channels used in the iterative process.

5. Retrieval results

The retrieval system outlined in the last section was used to produce fields of high-resolution satellite soundings for the 30 September 1980 case. The two sets of HIRS-2 measurements at 1000 and 1400 were analyzed independently, except for a common initial guess sounding composited from the 1200 RAOBs. The satellite-derived meteorological parameters were then compared quantitatively to conventional measurements at both the RAOB and surface observation scales. In addition, the satellite-derived water vapor fields were compared qualitatively to fields of moisture estimated from conventional surface measurements. Changes in the fields over the 4-hour time span were also examined.

a. Satellite–RAOB comparisons

As mentioned previously, the RAOBs were only available at 1200, midway between the two satellite passes at approximately 1000 and 1400. For this reason comparison of satellite-derived values to conventional RAOB measurements includes a time separation of 2 hours. Of the 27 RAOBs in the initial guess profile, those within 150 km of a satellite measurement position were used for this comparison. However, because of limitations on the satellite data availability due to calibration gaps and clouds, only 17 and 12 satellite–RAOB pairs were available at 1000 and 1400, respectively. The lower number of pairs at 1400 is due to extensive cloudiness at that time.

The results of the satellite–RAOB comparisons are shown in Table 5.1. Comparisons of the 1200 RAOBs to the 1000 and 1400 satellite-derived parameters at several standard levels are given separately by means of correlation coefficients, mean differences (biases), and rms differences.

Many of the satellite–RAOB comparisons show high correlations. (The square of the correlation coefficient represents the proportion of the variance in one set of measurements which can be explained by the other set of measurements, i.e., the explained variance.) For the retrieved temperatures the correlations with RAOB temperatures only fall below 0.60 (36% explained variance) at and above 30 kPa. This is due to the use of only the more transparent CO_2 channels in the retrieval

TABLE 5.1. Satellite–RAOB comparisons.

	1000 versus 1200 GMT			1400 versus 1200 GMT		
Parameter	Correl.	Bias	rms Diff.	Correl.	Bias	rms Diff.
Temperatures (°C):						
Surface	(0.62)	0.1	3.0	(0.60)	6.6	7.2
85 kPa	(0.88)	3.2	4.6	(0.82)	4.0	6.5
70 kPa	(0.71)	5.2	6.7	(0.72)	5.8	7.9
50 kPa	(0.91)	4.9	5.7	(0.94)	5.6	6.8
40 kPa	(0.84)	2.4	3.9	(0.83)	3.8	5.6
30 kPa	(0.62)	1.6	3.8	(0.48)	3.7	5.8
20 kPa	(−0.09)	−0.7	7.8	(0.38)	−0.4	9.9
Rad. sfc temp (°C)	(0.57)	−4.1	4.8	(0.63)	4.1	5.1
Total PW (mm)	(0.66)	3.4	4.8	(0.72)	4.8	6.5
Dew point temp (°C):						
Surface	(0.55)	−3.2	4.4	(0.46)	2.9	5.3
85 kPa	(0.34)	3.6	10.1	(0.33)	5.1	9.2
70 kPa	(0.31)	7.9	10.9	(0.36)	6.5	10.7
50 kPa	(0.28)	8.2	9.9	(0.05)	8.8	10.3

process. The highest temperature correlations occur at 50 kPa. Mean temperature differences (biases) are quite large and positive at all but 20 kPa. No attempt was made to eliminate these biases. Using similar measurements Phillips *et al.* (1979) and Schlatter (1981) obtained biases of about 1 K except near the surface. A much larger positive bias near the surface at 1400 shows the effect of increased surface heating after sunrise. Large rms differences are probably a result of instability in the combined moisture–temperature feedback, as well as the time difference between the two sets of measurements.

The radiative surface temperature is the value derived from the satellite window channels. The biases for the radiative surface temperature are negative and positive for 1000 and 1400, respectively. Diurnal changes explain why the radiative surface temperature is lower before sunrise (1000) and higher after sunrise (1400), creating the negative and positive biases.

The moisture comparisons show the highest correlations for the total precipitable water. The positive total water biases are probably linked to the positive temperature biases. An overestimation of temperatures will lead to an overestimation in moisture, and vice versa. Root-mean-square precipitable water differences are 4.8 and 6.5 mm at 1000 and 1400, respectively. For a mean total water of 25 mm these rms values represent 19 and 26% of the mean, respectively.

Although the dew point temperature comparisons show lower correlations than those for temperatures, the highest correlations are at the surface where more water typically resides. Biases are again positive except for the surface dew points at 1000. These values are strongly linked to the surface temperatures because at 1000 saturation occurred at the surface at many retrieval locations. Root-mean-square differences are 4.4 and 5.3 K, respectively, for the surface dew points in the two comparisons.

Considering these large rms differences and biases, the solution procedure is not optimized for error reduction. For the nocturnal inversion situations under study, the vertical atmospheric structure is highly variable near the surface. This proves to be a difficult task for the satellite sounder, especially without the use of surface observations. These quantitative comparisons should therefore not be considered as state of the art. Later comparisons will show that satellites can detect spatial features (gradients) comparable to those given by high density surface observations.

b. Satellite–surface observation comparisons

The conventional synoptic surface observations, as mentioned before, were used only for verification of the satellite-derived surface parameters. The typical synoptic surface observation spacing is approximately 100 km. The satellite-derived surface parameters, on the other hand, can be separated by as little as ~30 km. However, for comparison purposes the satellite soundings were retrieved at the same approximate density as the surface observations.

In order to compare the nonsynoptic satellite-derived values with the surface observations taken at synoptic times, the synoptic surface observations were linearly interpolated in time to both 1000 and 1400. Because not all observing stations reported at each synoptic time, there are fewer interpolated values than measured values at the surrounding synoptic times; there are 94 and 112 interpolated observations at 1000 and 1400, respectively.

For each of the time-interpolated observations the closest satellite-derived value was chosen for comparison. The only limitation was that the satellite value had to be within 60 km of the synoptic station. For this reason, and since the satellite-derived values were sometimes unavailable, the number of satellite–conventional pairs was reduced to 75 and 63 at 1000 and 1400, respectively.

The three surface variables which were compared are the temperature, the dew point temperature, and the relative humidity, with results shown in Table 5.2. Also shown is a comparison of the satellite-derived total precipitable water versus the precipitable water estimated from the surface dew point temperatures. Separate columns are used to give the satellite-versus-surface correlation coefficients, mean differences (biases), and rms differences at both 1000 and 1400. In the retrieval process no special attempt was made to eliminate a bias in the satellite-retrieved parameters. A positive bias, for example, indicates that the satellite-derived values are larger than the conventional values and vice versa.

As in the case of the satellite–RAOB comparison, the rms differences are the standard "error" analyses which are typically shown in most satellite–conventional comparisons. This difference is not entirely an error in the satellite products but is composed of errors in both the satellite and conventional data and discrepancies due to different space and time sampling methods between the two sets of measurements. Bruce

TABLE 5.2. Satellite–synoptic surface observation comparisons.

	1000 GMT (75 pairs)			1400 GMT (63 pairs)		
Parameter	Correl.	Bias	rms Diff.	Correl.	Bias	rms Diff.
Surface temperature (°C)	(0.53)	−4.5	5.2	(0.75)	−0.4	2.0
Surface dew point temp. (°C)	(0.59)	−3.0	4.2	(0.59)	1.8	4.4
Surface rel. humidity (%)	(0.19)	−8.9	21.0	(0.33)	−5.8	24.7
Estimated total PW (mm)	(0.34)	0.2	5.5	(0.62)	1.8	5.2

et al. (1977) found that rms temperature differences with a minimum of ~1 K can be attributed to the comparison of point versus area-averaged temperatures.

The correlation coefficients for surface temperature and surface dew point comparisons range from 0.53 to 0.75. The highest correlation of 0.75 represents a 56% explained variance using satellite retrievals to predict surface temperatures.

The last row in Table 5.2 shows a comparison of the satellite-derived precipitable water with the precipitable water estimated from the synoptic surface dew point values. The estimated total water values were obtained by the application of Eq. (3.2) to the surface dew points. The higher correlation at 1400 than at 1000 is probably the result of inversion breakup and vertical mixing after sunrise. Biases are less than 2 mm and rms differences are similar to those for the satellite–RAOB comparisons. The rms values of 5.5 and 5.2 mm are 22 and 21%, respectively, of the previously-used mean precipitable water of 25 mm.

1) A CLOSER LOOK AT 1000 GMT

The satellite-derived total water field at 1000 at the scale of the surface observation is plotted in Fig. 5.1a (contours are a result of subjective analysis). The analysis area is the smaller area in Fig. 3.1. More detail arises at this higher resolution than would appear at the RAOB scale. Outstanding features include a local moisture minimum in Illinois. At this resolution the moisture minimum is separated from the dry region to the west, whereas at the RAOB scale (Fig. 3.3a) the contours were drawn to indicate a dry tongue extending from Nebraska into Illinois. Other features include a moisture maximum in Arkansas and a strong moisture gradient from Arkansas into Missouri.

For comparison purposes, precipitable water has been estimated from the time-interpolated surface observations at 1000 by using Eq. (3.2) and is shown in Fig. 5.1b. Here the contours show a general moisture gradient from southeast to northwest. Dry regions to the west and over Illinois are separated by a thin moist

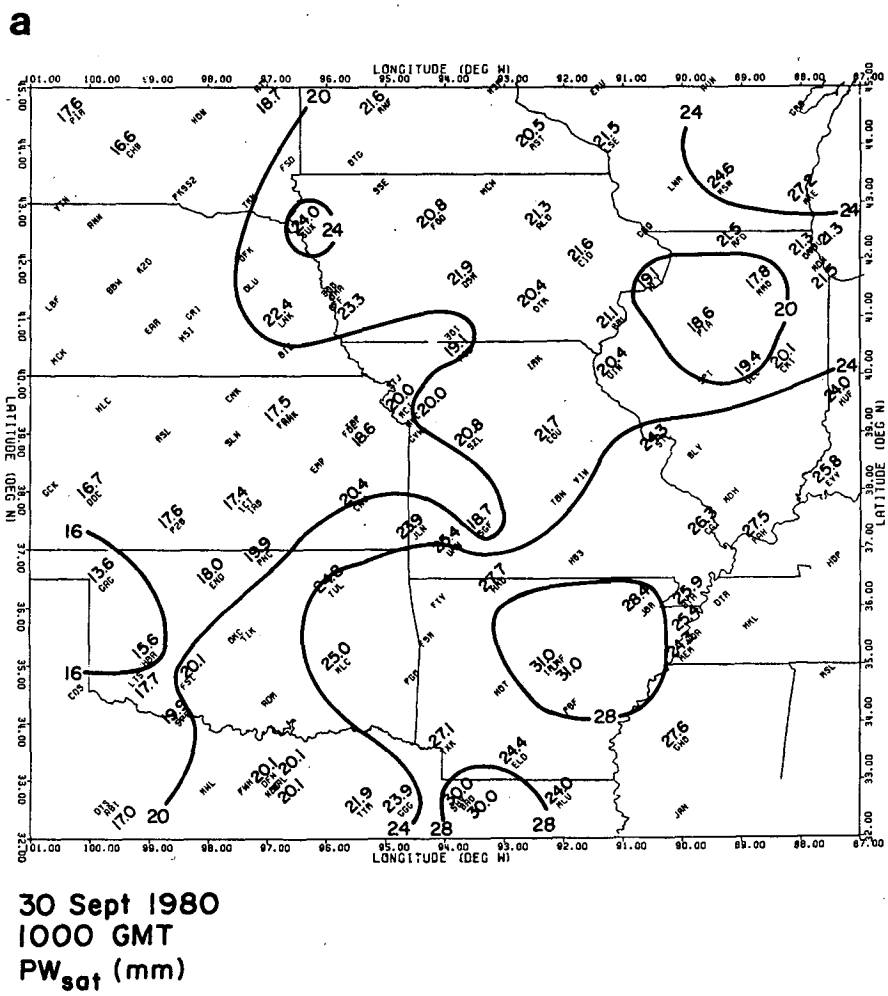

FIG. 5.1a. Satellite-derived total precipitable water (mm) at surface observation resolution for 1000 GMT 30 September 1980.

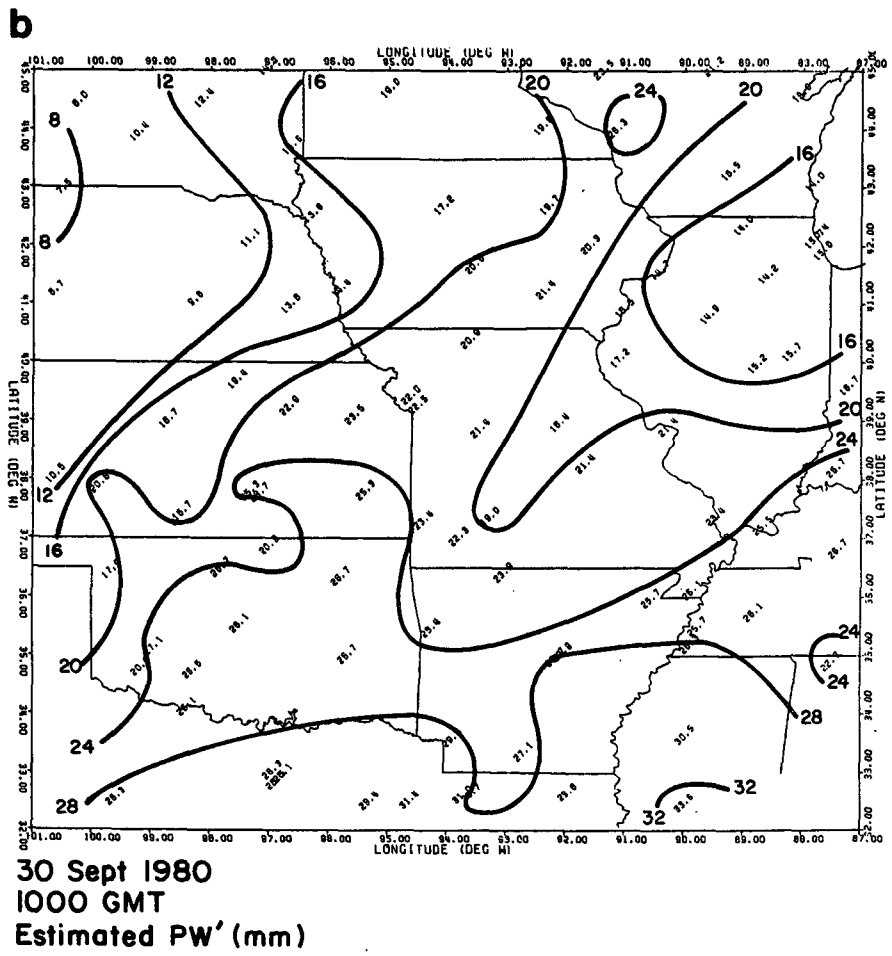

FIG. 5.1b. Total precipitable water (mm) estimated from time-interpolated surface observations at 1000 GMT 30 September 1980 by using Eq. (3.2).

region of as little as 100 km in width. This moist bridge agrees somewhat with the satellite-derived precipitable water field, which shows the dry tongue not linked from west to east. On the other hand, the satellite-derived moisture is greater over Arkansas than in the surface-estimated water contours, but weaker over Kansas. Differences will exist because of the nature of the two sets of measurements.

Figure 5.1c shows the difference field created when the surface-estimated precipitable water values are subtracted from the satellite-derived values. Because the estimated total moisture is determined by the surface dew point, it represents a certain moisture lapse rate or a given decrease in moisture with height. The satellite-derived moisture profile begins with a given initial-guess moisture profile and is adjusted to try to represent the true moisture distribution. If the satellite provides a better representation of the vertical moisture structure, then the satellite-minus-estimated difference will show something about the vertical extent of the moisture. This would be similar in interpretation to the actual-minus-estimated total moisture differences plotted at the RAOB locations in Fig. 3.3b. Positive differences represent regions where the atmosphere is determined by the satellite to be moist aloft, i.e., more moisture is detected than is estimated from the surface. On the other hand, negative differences represent regions where the atmosphere is dry aloft, i.e., less moisture is detected than is estimated from the surface.

Regions with the largest positive differences in Fig. 5.1c cover parts of Wisconsin and northern Illinois, parts of Nebraska and also parts of Arkansas. Here the moisture is detected by the satellite to be deeper than that suggested by a moisture profile estimated from the surface dew point. Negative values reach a maximum in Texas and Oklahoma with negative values extending into Iowa. Not surprisingly, this is also where the fog, shown in the 1400 visible image in Fig. 2.3a, forms. Regions where the atmosphere is moist aloft, such as over Arkansas, are not conducive to radiation fog development, even though lower layers of the atmosphere may be very moist, because infrared cooling to space is suppressed.

Following are two examples which serve to compare precipitable water amounts based on three determinations; an *in situ* sounding, a moisture profile esti-

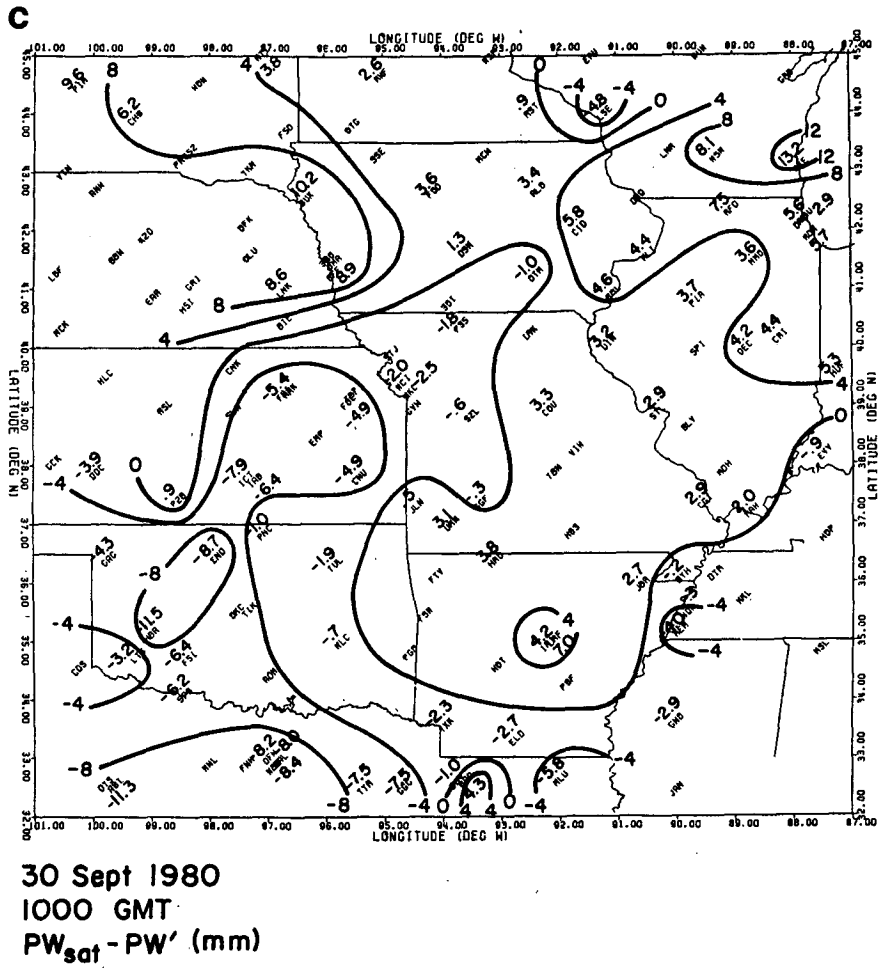

FIG. 5.1c. Difference between satellite-derived and surface-estimated total precipitable water (mm) at 1000 GMT 30 September 1980.

mated from a surface dew point measurement, and a satellite-derived moisture profile. The two examples are from regions of negative and positive differences between the satellite-derived and surface-estimated total water, respectively.

Examples of satellite and conventional soundings in a negative region are shown in Fig. 5.2a. Here the satellite sounding at 1000 is compared to the 1200 RAOB at Topeka (TOP). Also shown is a power-law moisture profile generated using Eq. (3.3), with the exponent determined by Eqs. (3.2) and (3.6). Because the atmosphere is dry above a shallow moist layer, the power-law moisture profile overestimates the moisture at most levels other than near the surface. The satellite-derived profile also overestimates the moisture at most levels except near the surface, but to a lesser degree than the surface-estimated moisture profile. Thus, a negative (satellite-minus-estimated) difference is determined for this case.

Figure 5.2b shows a similar comparison of moisture profiles for a positive region in Fig. 5.1c. Here surface-estimated and satellite-derived moisture profiles are compared to the 1200 Peoria (PIA) RAOB. In this case the surface-estimated moisture profile underestimates the actual moisture in the deep moist layer near the surface. The satellite-derived profile, on the other hand, more closely represents this deep moisture near the surface. The positive difference for the satellite-derived minus surface-estimated total water indicates a moist-aloft situation, or in this case a situation where the moisture is deeper than in the previous example.

In both of these examples, one each from a region of negative and positive difference, the satellite did provide a better moisture profile than that estimated from the surface dew point temperature. By comparison of satellite-derived total water to the surface-estimated moisture, which is of little value alone, there is an indication of vertical moisture structure, if only in terms of moisture depth. This is important in that only a few types of moisture profiles are meteorologically significant. Of basic importance in this case of fog formation is the vertical moisture extent. The neg-

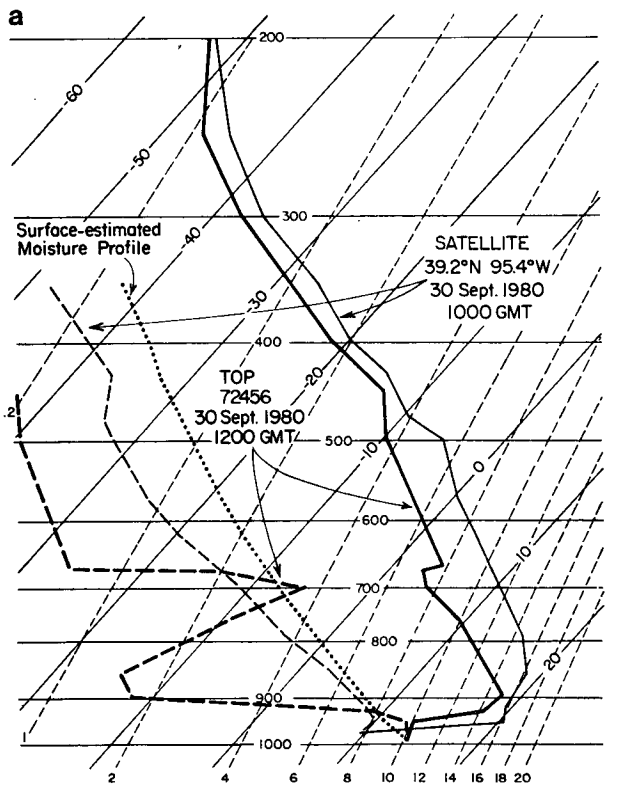

FIG. 5.2a. Topeka, Kansas RAOB at 1200 GMT 30 September 1980 showing a shallow moist layer near the surface. Dotted line is a power-law moisture profile based on the RAOB surface dew point temperature. (See text for further explanation.) Also plotted is the nearest satellite sounding at 1000 GMT, which does not contain the vertical detail of the RAOB but which better approximates the dry-over-moist situation.

ative values of satellite-derived minus surface-estimated moisture indicate a dry-over-moist situation for a large portion of the area where the radiation fog forms.

2) FOUR-HOUR TIME CHANGES

One goal of this study was to examine the satellite-derived moisture values to determine whether moisture variations could be detected at both high space and time resolutions. Toward this goal, the satellite-derived precipitable water field was generated for the 1400 satellite pass, as was previously done for 1000. The 4-hour time change in satellite-derived total precipitable water between 1000 and 1400 is plotted in Fig. 5.3a. Outstanding features include a large increase in moisture along the Iowa–Illinois border and an equally strong decrease in moisture in the vicinity of northeastern Nebraska. Negative values dominated a region extending from Nebraska into Kansas and Arkansas.

A similar time-change analysis of the surface-estimated total precipitable water is shown in Fig. 5.3b. Here, the same two features exist. The large increase in moisture, however, covers most of Illinois, approximately the region covered by weaker increases in the satellite-derived field in Fig. 5.3a. The region of strong negative values covers most of Kansas and spreads north and south. This is approximately the same region of maximum moisture decrease shown by the satellite-derived time change field. However, the largest negative values in Fig. 5.3b are now in Kansas and not Nebraska. The shift of the local maxima and minima between the two fields is related to the depth over which the moisture change occurs. The surface-estimated total water values more closely show surface moisture change, and the satellite-derived values show integrated moisture change.

A key to the reason why these satellite-derived moisture changes are reasonable is found by looking at the 70 kPa winds at 1200. Benwell (1965) used 70 kPa wind trajectories to compare advected moisture fields to those observed at a later time. His conclusion was that precipitable water is a fairly conservative quantity which could be advected with the 70 kPa winds. For this case the 70 kPa wind and streamlines are drawn in Fig. 5.4. The flow is generally from the north-north-

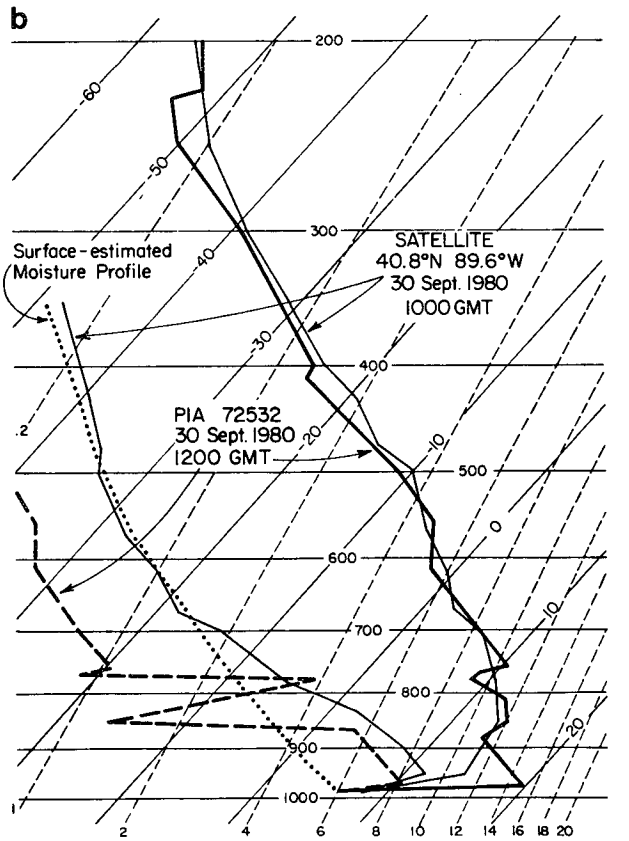

FIG. 5.2b. Peoria, Illinois RAOB at 1200 GMT 30 September 1980 with a deep moist layer near the surface. Dotted line is a power-law moisture profile based on the RAOB surface dew point temperature. (See text for further explanation.) Also plotted is the nearest satellite sounding at 1000 GMT with its better reconstruction of the low-level moisture.

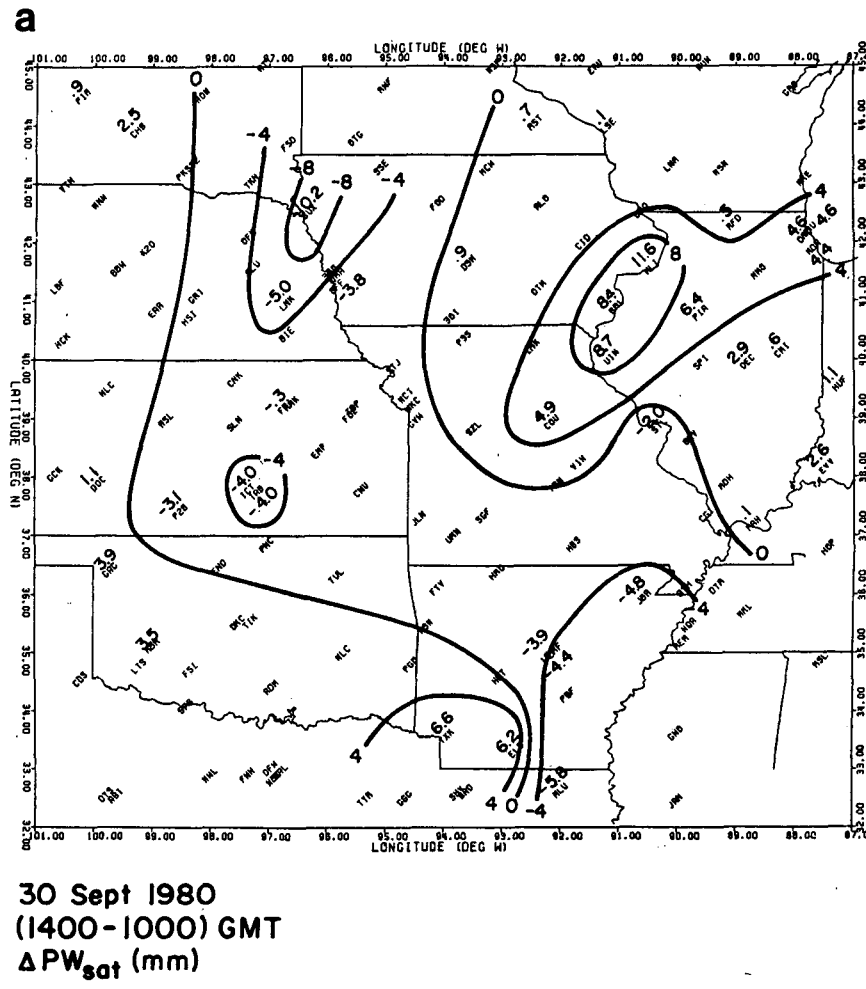

FIG. 5.3a. Four-hour time change in satellite-derived total precipitable water (mm), at surface observation scale, between 1000 and 1400 GMT 30 September 1980.

west, with a cyclonic pattern forming in the southeastern United States. Using this flow pattern along with the RAOB total precipitable water pattern in Fig. 3.3b, it is reasonable that moist air has been advected from Minnesota and Wisconsin into the previously dry slot in Iowa and Illinois. Also, the decrease in moisture in Kansas is likely associated with the advection of dry air from Colorado and western Nebraska toward the southeast.

Another possible reason for the increase in moisture in the Iowa–Illinois region may be low-level convergence causing moist air to be advected vertically from the surface. The surface wind analysis at 1200 (not shown) indicates some low-level convergence of moisture although the winds are weak (typically less than 5 m s^{-1}). This additional explanation is plausible because of the limited ability of midlevel (70 kPa) moisture advection alone, to explain the large (8+ mm) satellite-derived moisture increase in this region in only 4 hours.

6. Summary and conclusions

A physical, iterative retrieval scheme to derive meteorological parameters from satellite radiances has been developed. Of major interest is the ability to derive moisture parameters and to use these parameters in a mesoscale or high-resolution situation. The satellite-derived meteorological parameters were compared to conventional data at two scales. Comparisons were both quantitative, in which satellite-derived parameters were compared to the equivalent conventional parameters by means of correlation coefficients and mean and rms differences; and qualitative, in which fields of total precipitable water from the two data sets were compared and contrasted. Time-differencing was used to show the ability to obtain mesoscale moisture changes in time as well as space.

The meteorological situation studied involved the development of radiation fog which formed in an area where both sufficient moisture and nocturnal cooling

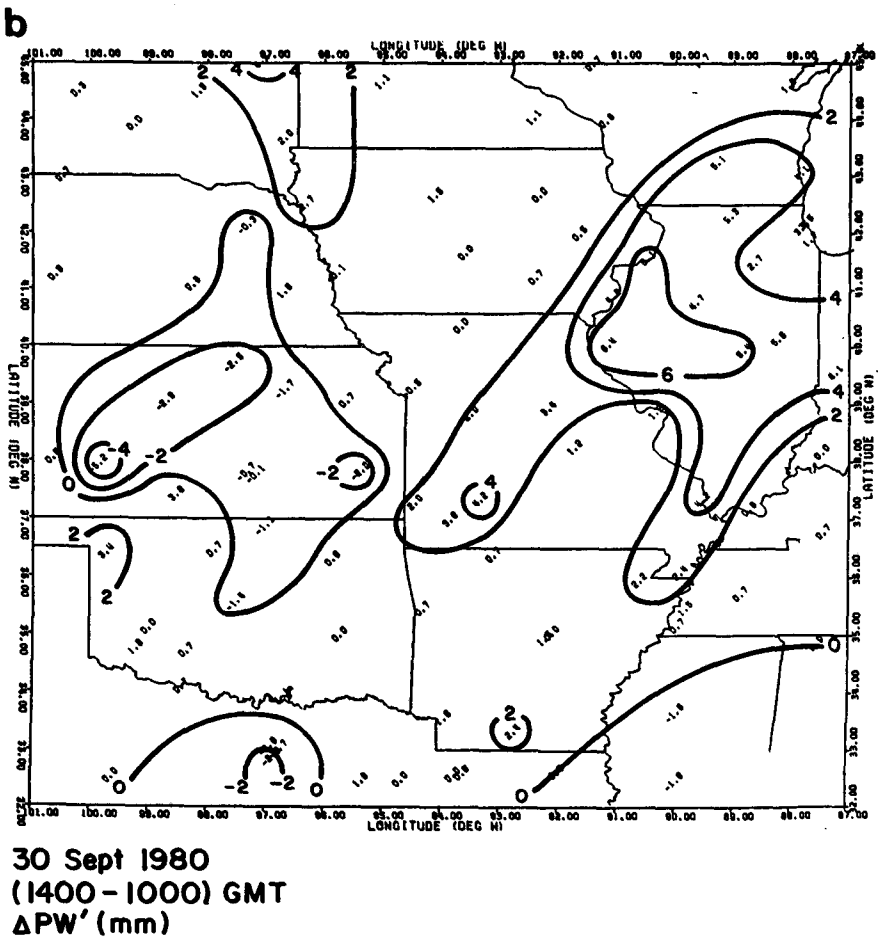

FIG. 5.3b. Four-hour time change in surface-estimated total precipitable water (mm) between 1000 and 1400 GMT 30 September 1980.

occurred. Surrounding regions contained either too little moisture for saturation, or moisture which was too deep for sufficient radiative cooling to occur.

The availability of the satellite data at 1000 and 1400 GMT from two polar-orbiting satellites presented the challenge of having to do retrievals both before and after sunrise, respectively. The main retrieval problem was caused by the existence of a surface temperature inversion over most of the area under study. The physical, iterative retrieval scheme was best able to handle this type of situation by allowing the surface skin temperature to float free of the temperature profile above the surface. With this method, either temperature inversions or superadiabatic layers at the surface can be added to the temperature profiles. This in effect adds vertical resolution to the retrieved soundings.

Another reason for recognizing the existence of a surface temperature inversion involves the satellite moisture retrieval capabilities. In a noninversion case the integrated radiances in a water vapor absorption band typically *decrease* with increasing moisture. However, when a temperature inversion exists at the surface the integrated radiance can *increase* with increasing atmospheric moisture. By calculating the moisture feedback values for the situation under study, the effect of the temperature inversion can be taken into account. For inversion cases the moisture feedback is typically reversed in sign and changed in magnitude from noninversion cases.

Three significant points were obtained from the comparisons at the higher resolution of the surface observations. First, the increased data density for the satellite-derived values show that small scale features can remain undetected by observations at only the RAOB scale. Secondly, differences between the satellite-derived and surface-estimated total water can indicate regions where the atmosphere is dry or moist aloft, or alternately can indicate the vertical moisture depth. The third point arises from a comparison of the 4-hour time change field from the satellite with a similar field from conventional sources. The comparison shows that the satellite is able to pick up temporal moisture changes which were similar in pattern to those estimated by the surface observations. The time change

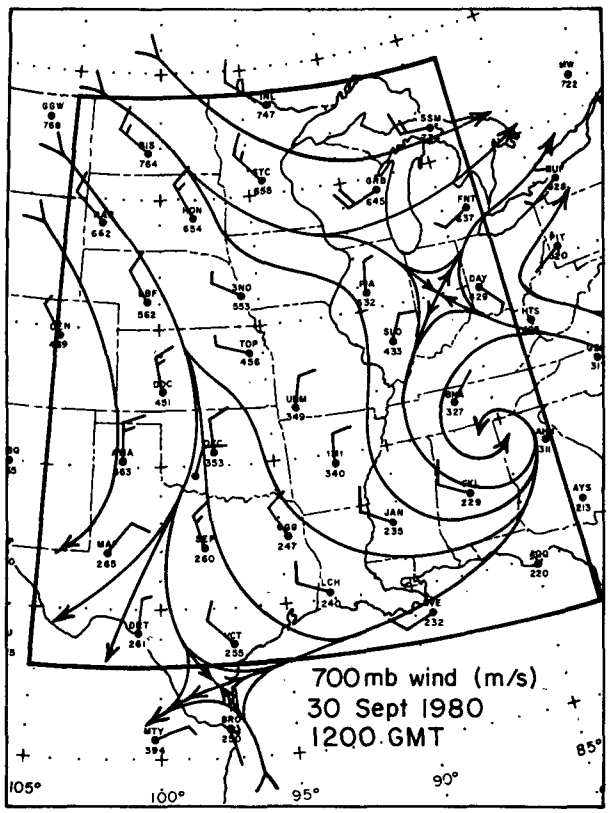

FIG. 5.4. Winds and streamlines at 70 kPa for RAOBs at 1200 GMT 30 September 1980. One full barb equals 10 m s^{-1}.

fields were reasonable when both advection of moisture and moisture convergence were considered. Using 70 kPa streamlines the flow of moisture from both dry to moist and moist to dry regions could in part explain the major changes which occurred. Surface moisture convergence also can be used to explain the time-increase in moisture detected by the satellite.

As this study shows, the satellite can detect sub-RAOB scale features due to its high-resolution capabilities. In addition, the satellite sounder is capable of detecting mesoscale moisture tendencies over the relatively short time span examined in this study. This capability will be enhanced with a time resolution of up to one-half hour with the advent of geosynchronous sounders like VAS.

One of the applications for high space and time resolution moisture fields from satellites is in the analysis and forecasting of severe weather. Such measurements would be especially useful in analyzing the pre-convective situation for moisture tendencies relating to later convective development. In such studies the moisture information is of great importance because of its large role in the energy processes relating to storm development.

Acknowledgments. Dr. C. M. Hayden and others of the NESDIS branch at the University of Wisconsin provided both the calibrated and earth-located TOVS data and TOVS transmittance software used in this study. RAOB and surface data were obtained from the NCAR data base through the help of Paul Mulder. Satellite imagery was provided by Judith Bonds of the Bureau of Reclamation in Denver.

The author also recognizes the constructive reviews of his dissertation provided by Drs. Thomas H. Vonder Haar, Thomas B. McKee, William R. Cotton and Frank R. DeMeyer, as well as Mr. Alan Lipton. This publication is based on and derived from that work.

Typing of the manuscript was done by Robin Wilson. Drafting, other than computer graphics, was performed by Judy Sorbie. Streamlines were drawn by Jim Toth.

Funding for this work was provided AFGL Contract AF19628-80-C-0140.

APPENDIX

Numerical Calculation of Moisture Feedback Conversion Factors

In order to explicitly add the effect of a temperature inversion into the moisture feedback, it was necessary to modify the feedback equation originally developed by Smith (1970). The modifications given here are an extension of Smith's development (see also Smith and Howell, 1971) and are necessary due to numerical integration by computer.

Starting from Eq. (13) of Smith (1970), the equivalent integral for S_k is

$$S_k^{-1} = \int_0^{p_{\max}} U(p) \frac{\delta\tau_k(p)}{\delta U(p)} \delta L[k, T(p)], \quad \text{(A1)}$$

where $U(p)$ is the precipitable water integrated to pressure level p, $\tau(p)$ is the transmittance to level p, and L is the Planck function of wavenumber k and temperature T.

In summation form, Eq. (A1) becomes

$$S_k^{-1} = \sum_{m=1}^{\max-1} \bar{U}_m \Delta\tau_{k,m} \Delta L_{k,m} \Delta U_m^{-1}, \quad \text{(A2)}$$

where

$$\bar{U}_m = \frac{1}{2}[U(p_m) + U(p_{m+1})],$$

$$\Delta\tau_{k,m} = \tau_{k,m} - \tau_{k,m+1},$$

$$\Delta L_{k,m} = L[k, T(p_{m+1})] - L[k, T(p_m)],$$

$$\Delta U_m = U(p_{m+1}) - U(p_m).$$

The precipitable water increases with pressure by definition, since it is integrated downward:

$$U(p) = g^{-1} \int_0^p Q(p)\delta p, \quad \text{(A3)}$$

where $Q(p)$ is the mixing ratio profile. Therefore ΔU is positive. Likewise $\Delta\tau$ is positive since the transmittance τ decreases with pressure (increasing m). The remaining term ΔL is also positive if temperature T increases with pressure. However, this is not always the case. When a temperature inversion exists at the surface, then $T_{sfc} < T_{max}$.

In order to account for the strong effect of a lowered surface temperature upon the integrated radiance (as in Fig. 4.4) a term similar to the surface term in the radiative transfer equation has been added to Eq. (A2):

$$S_k^{-1} = S_k^{-1} + \tau_{k,max}\Delta L_{k,sfc}, \qquad \text{(A4)}$$

where

$$\Delta L_{k,sfc} = L(k, T_{sfc}) - L(k, T_{max}).$$

This term will be negative for $T_{sfc} < T_{max}$, so it will reduce the magnitude of S^{-1}, or even cause it to become negative. This is especially likely for the most transparent channel since the surface transmittance $\tau_{k,sfc}$ can be large. If S^{-1} is negative then the reverse effect of increased radiance with increased precipitable water can be simulated. Empirical testing has shown that this actually happens. Unfortunately, the S^{-1} term can approach zero causing S to approach infinity. This possibility is eliminated by forcing S to zero as S^{-1} approaches zero, in such a way that the mapping is continuous. The reasoning is that as S^{-1} approaches zero, the direction of the moisture feedback becomes uncertain. By forcing S to zero in these cases the uncertainty is not carried over into large feedback but is diminished in magnitude. As a result of empirical testing, if $S^{-1} < 4$, then $S = S^{-1}/16$, is used. Values larger than $S = 0.25$ (25%) cause too much moisture feedback. The units of S are inverse radiance units.

REFERENCES

Benwell, G. R. R., 1965: The estimation and variability of precipitable water. *Meteor. Mag.*, **94,** 319–327.

Bolsenga, S. J., 1965: The relationship between total atmospheric water vapor and surface dew point on a mean daily and hourly basis. *J. Appl. Meteor.*, **4,** 430–432.

Bruce, R. E., L. D. Duncan and J. H. Pierluissi, 1977: Experimental study of the relationship between radiosonde temperatures and satellite-derived temperatures. *Mon. Wea. Rev.*, **105,** 493–496.

Chesters, D., L. W. Uccellini and A. Mostek, 1982: VISSR atmospheric sounder (VAS) simulation experiment for a severe storm environment. *Mon. Wea. Rev.*, **110,** 198–216.

Gruber, A., and C. D. Watkins, 1979: Preliminary evaluation of initial atmospheric moisture from the TIROS-N sounding system. *Satellite Hydrology, Proc. Fifth Ann. Symp. Remote Sensing,* Minneapolis, Amer. Water Resourc. Assoc., 115–123.

Gurka, J., 1976: Using satellite data as an aid to forecasting fog and stratus formation. NWS/NESS Satellite Applications Information Note 3/76-1, AWS/TN-79/003 (compiled 1979), 47–51. [Available from Air Weather Service, Scott AFB, IL.]

Hayden, C. M., W. L. Smith and H. M. Woolf, 1981: Determination of moisture from NOAA polar orbiting satellite sounding radiances. *J. Appl. Meteor.*, **20,** 450–466.

Hillger, D. W., 1983: Mesoscale moisture fields retrieved from satellite infrared radiances in nocturnal inversion cases. Ph.D. dissertation, Dept. Atmos. Sci., Colorado State University, Fort Collins, 140 pp. [Available from University Microfilms, Ann Arbor, MI].

——, and T. H. Vonder Haar, 1981: Retrieval and use of high-resolution moisture and stability fields from Nimbus-6 HIRS radiances in pre-convective situations. *Mon. Wea. Rev.*, **109,** 1788–1806.

Lipton, A. E., and D. W. Hillger, 1982: Objective analysis of discontinuous satellite-derived data fields for grid point interpolation., *J. Appl. Meteor.*, **21,** 1571–1581.

Moyer, V., J. R. Scoggins, N. M. Chou and G. S. Wilson, 1978: Atmospheric structure deduced from routine Nimbus-6 satellite data. *Mon. Wea. Rev.*, **106,** 1340–1352.

Parmenter, F. C., 1976: Low-level moisture intrusion from infrared imagery. *Mon. Wea. Rev.*, **104,** 100–104.

Paulson, B. A., and L. H. Horn, 1981: Nimbus-6 temperature soundings obtained using interactive video-graphics computer techniques. *Bull. Amer. Meteor. Soc.*, **62,** 1308–1318.

Phillips, N., L. McMillin, A. Gruber and D. Wark, 1979: An evaluation of early operational temperature soundings from TIROS-N. *Bull. Amer. Meteor. Soc.*, **60,** 1188–1197.

Reitan, C. H., 1963: Surface dew point and water vapor aloft. *J. Appl. Meteor.*, **2,** 776–779.

Schlatter, T. W., 1981: An assessment of operational TIROS-N temperature retrievals over the United States. *Mon. Wea. Rev.*, **109,** 110–119.

Schwalb, A., 1978: The TIROS-N/NOAA A–G satellite series. NOAA Tech. Memo. NESS 95, 75 pp. [NTIS PB-283859].

Smith, W. L., 1966: Note on the relationship between total precipitable water and surface dew point. *J. Appl. Meteor.*, **5,** 726–727.

——, 1970: Iterative solution of the radiative transfer equation for the temperature and absorbing gas profile of an atmosphere. *Appl. Opt.*, **9,** 1993–1999.

——, and H. B. Howell, 1971: Vertical distribution of atmospheric water vapor from satellite infrared spectrometer measurements. *J. Appl. Meteor.*, **10,** 1026–1034.

——, C. M. Hayden, H. M. Woolf, H. B. Howell and F. W. Nagle, 1979a: Satellite sounding applications to mesoscale meteorology. *Proc. Symp. Remote Sounding of the Atmosphere from Space,* Innsbruck, COSPAR, Pergamon, 33–47.

——, H. M. Woolf, C. M. Hayden, D. Q. Wark and L. M. McMillin, 1979b: The TIROS-N operational vertical sounder. *Bull. Amer. Meteor. Soc.*, **60,** 1177–1187.

——, V. E. Suomi, W. P. Menzel, H. M. Woolf, L. A. Sromovsky, H. E. Revercomb, C. M. Hayden, D. N. Erickson and F. R. Mosher, 1981: First sounding results from VAS-D. *Bull. Amer. Meteor. Soc.*, **62,** 232–236.

Wark, D. Q., J. H. Leinesch and M. P. Weinreb, 1974: Satellite observations of atmospheric water vapor. *Appl. Opt.*, **13,** 507–511.

Weinreb, M. P., H. E. Fleming, L. M. McMillin and A. C. Neuendorffer, 1981: Transmittances for the TIROS Operational Vertical Sounder. NOAA Tech. Rep. NESS 85, 60 pp. [NTIS PB82-155920].